Journal Name

ARTICLE

# Azobenzene molecular glasses with tuned glass transition temperatures: from optimal light-induced motion to self-erasable gratings

Received 00th January 20xx,
Accepted 00th January 20xx

DOI: 10.1039/x0xx00000x

www.rsc.org/

Austin Diggins,[a] Eoin Dawson,[a] Mahnaz Kamaliardakani,[b] Christian Pellerin,*[,b] Ribal Georges Sabat*[,a] and Olivier Lebel*[,c]

The rate of photomechanical formation of surface relief gratings (SRG) in thin films of azobenzene materials depends on their glass transition temperature ($T_g$), with an optimal $T_g$ around 50-60 °C yielding the fastest SRG growth. Herein, the SRG growth of five analogous Disperse Red 1 molecular glasses with $T_g$ values ranging from 9 to 71 °C was studied with two different laser wavelengths (488 and 532 nm). It was found that the optimal $T_g$ for SRG growth increases with laser irradiance, from approximately 50 °C at 100 mW/cm$^2$ to over 70 °C at 300 mW/cm$^2$. Furthermore, the azobenzene glass with a sub-ambient $T_g$ of 9 °C can inscribe self-erasable gratings that collapse spontaneously when irradiation is stopped in a repeatable fashion, thereby paving the way for light-controlled optical devices.

## Introduction

Azobenzene and its derivatives are widely known for their unique photonic properties, which result in large part from the cis-trans isomerization of the central N=N bond.[1] Arguably, one of the most impressive outcomes of this isomerization is the photomechanical behavior of azobenzene-containing thin films, where exposure to an absorbing laser wavelength leads to repeated trans-cis-trans isomerization cycles which result in molecular mass transport within the material.[2] One of the most useful photomechanical manifestations in azobenzene materials is the formation of periodically ordered nanostructures, such as surface relief gratings (SRG), when exposed to a collimated laser beam interference pattern.[3] The laser light causes molecular migration from bright towards dark laser irradiance zones, thereby yielding a periodic pattern composed of grooves identical to the second derivative of the interference pattern.[4]

To inscribe SRG, the azo materials must be deposited as amorphous thin films, as the close packing in crystals hinders molecular movement.[5] As most azobenzene derivatives readily crystallize, the chromophores are typically incorporated into materials that can form amorphous thin films using a variety of deposition methods.[6] Polymers are the most commonly used supports, as they can readily form thin films, but small molecules offer several advantages linked to their monodisperse nature: they are easier to purify, characterize and process, and their properties are independent of chain length and dispersity, leading to higher batch homogeneity.[7-10] However, as small molecules tend to crystallize orders of magnitude faster than polymers, care must be exercised to design molecular materials that will form kinetically stable glassy phases rather than crystallizing.[11, 12] Such compounds are called molecular glasses, or amorphous molecular materials, and developments during the last thirty years have led to improved strategies for the design of small organic structures with extremely slow crystallization kinetics.[7-10] Azobenzene-containing molecular glasses have been synthesized with various structural elements that prevent their crystallization, including triarylamino groups,[13-21] triphenylmethyl groups,[22] or arylaminotriazine groups,[23] the latter of which is used in our research group. These materials can easily be synthesized in high yields using a modular approach from an azobenzene derivative with a functional group that can be covalently bonded to a glass-forming arylaminotriazine precursor. For example, commercially available Disperse Red 1 can be bonded to a triazine derivative with an amino group with a carbonylating reagent to form an adduct (gDR1) that combines the optical properties of the chromophore and the glass-forming properties of the triazine moiety.[24]

Though SRG formation and growth has been abundantly studied, few studies exist on SRG growth kinetics as a function of the glass transition temperature ($T_g$) of the material. Interestingly, Yager *et al.*[25] reported on the temperature dependence of the photomechanical effect in an azopolymer material with a $T_g$ of 95 °C and they found that the mass transport is driven by photoexpansion below a crossover temperature of 50 °C and by photocontraction above this temperature. Multiple other polymers containing azobenzene groups have been reported in the literature,[26] but as they use several different polymer backbones, it is difficult to establish reliable correlations as the structures of the materials can be

[a] *Department of Physics and Space Science, Royal Military College of Canada, PO Box 17000, Station Forces Kingston, Ontario CANADA, K7K 7B4. sabat@rmc.ca*
[b] *Département de chimie, Université de Montréal, C.P. 6128, succursale Centre-ville, Montréal, Québec, CANADA, H3C 3J7. c.pellerin@umontreal.ca*
[c] *Department of Chemistry and Chemical Engineering, Royal Military College of Canada, PO Box 17000, Station Forces Kingston, Ontario CANADA, K7K 7B4. Olivier.Lebel@rmc.ca*

† Footnotes relating to the title and/or authors should appear here.
Electronic Supplementary Information (ESI) available: DSC thermograms of the compounds reported herein, UV-Vis spectra of gDR1$_{Tg}$, and additional <P2>$_{res}$ data. See DOI: 10.1039/x0xx00000x

radically different. It is important that the structures of the materials remain analogous even though their $T_g$ has to be different. This problem was solved in a previous study by our group where gDR1 was blended with passive analogous molecular glass hosts.[27] Blends with $T_g$ values ranging from 19 to 88 °C were obtained by blending either 10 or 40 wt% gDR1 with host glasses with a wide range of $T_g$ values. The principal conclusions from that study were that the $T_g$ that led to the fastest SRG growth (at ambient temperature) was 60 °C, as materials with $T_g$ values that were too high were too rigid, thereby slowing the molecular migration, while materials with $T_g$ values that were too low were too soft to retain their molecular orientation and macroscopic features. However, the fact that the various blends contained 1) different gDR1 loadings, and 2) often low gDR1 loadings, may signify that the comparisons were not completely accurate.

A similar observation was made in a subsequent study, where a second gDR1 derivative with a lower $T_g$ value of 51 °C showed faster SRG growth than gDR1 with a $T_g$ of 71 °C.[28] For clarity, the various gDR1 materials will hereon be designated according to their glass transition temperature (**gDR1$_{Tg}$**).

In the present work, to study the impact of $T_g$ on SRG growth, we used our expertise in molecular glass engineering to design and synthesize three new gDR1 derivatives, thereby gaining access to a total of five analogous gDR1 derivatives with $T_g$ values ranging from 9 to 71 °C. The optimal $T_g$ for SRG growth was found to increase with laser irradiance, from approximately 50 °C at 100 mW/cm$^2$ to over 70 °C at 300 mW/cm$^2$, which is likely a consequence of photoplasticization upon irradiation. Moreover, the material with a sub-ambient $T_g$ of 9 °C was found to inscribe transient SRG that self-erase when laser irradiation is stopped, paving the way for light-controlled optical devices.

## Experimental Section

### General

2-Butylamino-4,6-dichloro-1,3,5-triazine[29] and 2-mexylamino-4,6-dichloro-1,3,5-triazine[30] were synthesized according to literature procedures. All other reagents and solvents were purchased from commercial sources and used without further purification. FTIR spectra were recorded with thin films cast from $CH_2Cl_2$ on KBr windows using a Perkin-Elmer Spectrum 65 spectrometer. UV-visible absorption spectra were acquired using a Hewlett-Packard 8453 spectrometer. $^1$H and $^{13}$C NMR spectra were recorded on a 400 MHz Bruker AV400 spectrometer at 363 K. Decomposition analyses of molecular glasses were obtained using a TGA 2950 thermogravimetric analyzer (TA Instruments) at a heating rate of 50 °C/min under a nitrogen atmosphere. $T_g$, $T_c$ and $T_m$ were recorded by DSC with a TA Instruments 2010 or a TA Instruments Q20 calorimeter calibrated with indium using a heating rate of 5 °C/min. Transition temperatures were reported after an initial cycle of heating and cooling.

### Synthesis

**Synthesis of 2-dibutylamino-4-(N-methylphenylamino)-6-chloro-1,3,5-triazine (1a).** To a solution of 2-dibutylamino-4,6-dichloro-1,3,5-triazine (7.00 g, 25.3 mmol) in acetone (50 mL) in a round-bottomed flask equipped with a magnetic stirrer was added $K_2CO_3$ (3.49 g, 25.3 mmol), then a solution of N-methylaniline (2.74 mL, 2.71 g, 25.3 mmol) in acetone (20 mL) was added dropwise at 0 °C. Once the addition complete, the mixture was stirred 2 h at ambient temperature, then the mixture was poured into $H_2O$ and stirred for 30 min. The solution was extracted with hexanes (3x). The combined organic extracts were washed with 1M aq. HCl, $H_2O$ and aq. $NaHCO_3$, dried over $Na_2SO_4$, filtered, and the volatiles were removed under reduced pressure to yield 7.60 g of the title compound as an oil (21.9 mmol, 87 %): FTIR ($CH_2Cl_2$/KBr) 3039, 2958, 2932, 2872, 2862, 1600, 1562, 1491, 1433, 1400, 1377, 1324, 1265, 1231, 1164, 1109, 1067, 970, 928, 802, 764, 735, 693 cm$^{-1}$; $^1$H NMR (400 MHz, $CDCl_3$, 298 K) δ 7.35 (t, *J* = 7.4 Hz, 2H), 7.25 (d, *J* = 7.3 Hz, 2H), 7.21 (t, *J* = 7.3 Hz, 1H), 3.46 (s, 3H), 3.46 (m, 2H), 3.22 (br m, 2H), 1.51 (m, *J* = 7.3 Hz, 2H), 1.39 (br m, 2H), 1.29 (m, *J* = 7.7 Hz, 2H), 1.11 (br m, 2H), 0.91 (t, *J* = 7.3 Hz, 3H), 0.80 (br m, 3H) ppm; $^{13}$C NMR (100 MHz, $CDCl_3$) δ 138.1, 164.4, 163.6, 143.5, 128.6, 126.5, 126.1, 46.6, 46.0, 29.4, 28.8, 19.4, 19.3, 13.6, 13.5 ppm; HRMS (ESI) m/z: $[M + Na]^+$ calcd. for $C_{18}H_{26}ClNaN_5$: 370.1769, found: 370.1772.

**Synthesis of 2-dibutylamino-4-mexylamino-6-chloro-1,3,5-triazine (1b).** Compound **1b** was synthesized from 2-butylamino-4,6-dichloro-1,3,5-triazine (7.0 g, 25.3 mmol) using the same procedure as dibutylamino analogue **1a** using 3,5-dimethylaniline (3.15 mL, 3.06 g, 25.3 mmol) instead of N-methylaniline. Yield: 51 %; $T_m$ 100 °C; FTIR ($CH_2Cl_2$/KBr) 3278, 3111, 2958, 2930, 2870, 2863, 1587, 1534, 1498, 1465, 1451, 1432, 1392, 1375, 1317, 1281, 1223, 1171, 1043, 985, 917, 839, 801, 684, 658 cm$^{-1}$; $^1$H NMR (400 MHz, $CDCl_3$, 298 K) δ 7.30 (s, 1H), 7.21 (s, s, 2H), 6.73 (s, 1H), 3.55 (q, *J* = 7.5 Hz, 4H), 2.31 (s, 6H), 1.61 (m, *J* = 6.7 Hz, 4H), 1.37 (m, *J* = 7.7 Hz, 4H), 0.96 (t, *J* = 7.3 Hz, 6H) ppm; $^{13}$C NMR (100 MHz, $CDCl_3$) δ 168.6, 164.5, 163.3, 138.3, 137.9, 125.2, 117.8, 47.6, 47.2, 29.8, 29.5, 21.4, 20.3, 20.0, 13.9, 13.8 ppm; HRMS (ESI) m/z: $[M + Na]^+$ calcd. for $C_{19}H_{28}ClNaN_5$: 384.1925, found: 384.1931.

**Synthesis of 2-pyrrolidinyl-4-mexylamino-6-chloro-1,3,5-triazine (1c).** To a solution of 2-mexylamino-4,6-dichloro-1,3,5-triazine (6.20 g, 23.0 mmol) in acetone (50 mL) in a round-bottomed flask equipped with a magnetic stirrer was added $K_2CO_3$ (3.18 g, 23.0 mmol), then a solution of pyrrolidine (1.92 mL, 1.64 g, 23.0 mmol) in acetone (20 mL) was added dropwise at 0 °C. Once the addition complete, the mixture was stirred 2 h at ambient temperature, then the mixture was poured into $H_2O$ and stirred for 30 min. The precipitate was collected by filtration, washed with $H_2O$ and hexanes. The crude product was recrystallized from hot toluene to yield 2.63 g of the title compound (8.66 mmol, 38 %): $T_m$ 168 °C; FTIR ($CH_2Cl_2$/KBr) 3271, 3229, 3188, 3108, 2971, 2950, 2918, 2876, 1590, 1534, 1496, 1477, 1451, 1391, 1338, 1276, 1238, 1172, 1124, 1051, 988, 841, 796 cm$^{-1}$; $^1$H NMR (400 MHz, $CDCl_3$, 298 K) δ 7.33 (s, 1H), 7.25 (s, 2H), 6.72 (s, 1H), 3.61 (m, 4H), 2.30 (s, 6H), 1.98 (m, 4H) ppm; $^{13}$C NMR (100 MHz, $CDCl_3$) δ 168.4, 163.1, 162.8, 138.3, 137.9, 125.1, 117.7, 46.6, 46.5, 24.1, 25.0, 21.4 ppm; HRMS (ESI) m/z: $[M + H]^+$ calcd. for $C_{15}H_{19}ClN_5$: 304.1324, found: 304.1328.

**Synthesis of 2-dibutylamino-4-(N-phenylamino)-6-piperazinyl-1,3,5-triazine (2a).** 2-Dibutylamino-4-(N-phenylamino)-6-chloro-1,3,5-triazine (**1a**) (4.0, 11.5 mmol) and piperazine (9.91 g, 115 mmol) were added in THF (50 mL) in a round-bottomed flask equipped with a magnetic stirrer and a water-jacketed condenser, then the mixture was heated at 80 °C for 18 h. After the mixture was allowed to cool down to room temperature, the unreacted ethylenediamine was evaporated under vacuum. The residue was dissolved in 1M aqueous HCl, and the precipitate was removed by filtration and washed with $H_2O$. NaOH pellets were added to the filtrate until the pH became basic (>12), then the mixture was stirred for 30 min, at which time the solvent was decanted. The precipitated product was dissolved in $CH_2Cl_2$, dried over $Na_2SO_4$, filtered, and the solvent was thoroughly evaporated under reduced pressure to yield 3.06 g of the title compound (7.69 mmol, 67 %): $T_g$ -29 °C; FTIR ($CH_2Cl_2$/KBr) 3301, 3060, 3033, 2955, 2930, 2870, 2855, 1601, 1545, 1529, 1491, 1438, 1390, 1313, 1287, 1263, 1204, 1108, 1051, 1008, 807, 763, 693 $cm^{-1}$; $^1H$ NMR (400 MHz, DMSO-$d_6$, 363 K) δ 7.32 (m, 4H), 7.14 (t, *J* = 4.4 Hz Hz, 1H), 3.57 (m, 4H), 3.40 (s, 3H), 3.38 (m, 4H), 2.68 (m, 4H), 1.48 (m, *J* = 7.1 Hz, 4H), 1.24 (m, *J* = 7.1 Hz, 4H), 0.87 (t, *J* = 7.3 Hz, 6H) ppm; $^{13}C$ NMR (100 MHz, DMSO-$d_6$) δ 164.9, 164.4, 164.3, 144.9, 127.9, 126.1, 124.4, 45.9, 45.4, 43.9, 36.6, 29.6, 19.5, 13.7 ppm; HRMS (ESI) m/z: $[M + H]^+$ calcd. for $C_{22}H_{36}N_7$: 398.3027, found: 398.3027.

**Synthesis of 2-dibutylamino-4-mexylamino-6-(2-aminoethylamino)-1,3,5-triazine (2b).** 2-Dibutylamino-4-mexylamino-6-chloro-1,3,5-triazine (**1b**) (4.0 g, 11.1 mmol) and ethylenediamine (10 mL) were added in a round-bottomed flask equipped with a magnetic stirrer and a water-jacketed condenser, then the mixture was heated at 80 °C for 18 h. After the mixture was allowed to cool down to room temperature, the unreacted ethylenediamine was evaporated under vacuum. The residue was dissolved in 1M aqueous HCl, and the precipitate was removed by filtration and washed with $H_2O$. NaOH pellets were added to the filtrate until the pH became basic (>12), then the mixture was stirred for 30 min, at which time the solvent was decanted. The precipitated product was dissolved in $CH_2Cl_2$, dried over $Na_2SO_4$, filtered, and the solvent was thoroughly evaporated under reduced pressure to yield 3.95 g of the title compound (10.2 mmol, 93 %): $T_g$ -3 °C; FTIR ($CH_2Cl_2$/KBr) 3282, 2956, 2927, 2870, 2858, 1588, 1540, 1516, 1427, 1370, 1313, 1198, 1176, 1098, 835, 808, 686 $cm^{-1}$; $^1H$ NMR (400 MHz, DMSO-$d_6$, 363 K) δ 8.28 (br s, 1H), 7.37 (s, 2H), 6.57 (s, 1H). 6.38 (br s, 1H), 3.80 (br s, 2H), 3.51 (t, *J* = 7.5 Hz, 4H), 3.39 (br m, 2H), 2.85 (t, *J* = 6.1 Hz, 2H), 2.23 (s, 6H), 1.58 (m, *J* = 7.2 Hz, 4H), 1.34 (m, *J* = 7.5 Hz, 4H), 0.93 (t, *J* = 7.4 Hz, 6H) ppm; $^{13}C$ NMR (100 MHz, DMSO-$d_6$) δ 165.5, 164.5, 163.8, 140.5, 136.8, 122.6, 116.9, 46.0, 41.7, 40.4, 29.7, 21.1, 19.6, 13.8 ppm; HRMS (ESI) m/z: $[M + H]^+$ calcd. for $C_{21}H_{36}N_7$: 386.3027, found: 386.3028.

**Synthesis of 2-pyrrolidinyl-4-mexylamino-6-(2-aminoethylamino)-1,3,5-triazine (2c).** Compound **2c** was synthesized using the same procedure as dibutylamino analogue **2b**. Yield: 76 %; $T_g$ 50 °C; FTIR ($CH_2Cl_2$/KBr) 3276, 3118, 2967, 2947, 2926, 2869, 1586, 1540, 1516, 1479, 1437, 1372, 1338, 1246, 1200, 1175, 1119, 911, 836, 808, 736, 687, 616 $cm^{-1}$; $^1H$ NMR (400 MHz, DMSO-$d_6$, 363 K) δ 8.32 (br s, 1H), 7.43 (s, 2H), 6.54 (s, 1H), 6.41 (br s, 1H), 3.50 (m, 4H), 3.37 (m, 2H), 2.81 (t, *J* = 6.0 Hz, 2H), 2.23 (s, 6H), 1.89 (m, 4H) ppm; $^{13}C$ NMR (100 MHz, DMSO-$d_6$) δ 165.6, 163.7, 163.2, 140.6, 136.9, 122.5, 117.0, 45.6, 42.2, 41.0, 24.8, 21.2 ppm; HRMS (ESI) m/z: $[M + H]^+$ calcd. for $C_{17}H_{26}N_7$: 328.2244, found: 328.2242.

**Synthesis of gDR1$_9$.** To a stirred suspension of N,N'-carbonyldiimidazole (0.773 g, 4.77 mmol) in dry DMF (7.5 mL) in a dry round-bottomed flask equipped with a magnetic stirrer was slowly added Disperse Red 1 (1.00 g, 3.18 mmol) in small portions at ambient temperature, then the mixture was stirred for 18 h under nitrogen atmosphere. The mixture was poured into $H_2O$, stirred 10 min, then the precipitate was collected by filtration and washed with copious amounts of $H_2O$. The crude residue was redissolved in THF (20 mL), then 2-dibutylamino-4-(N-phenylamino)-6-piperazinyl-1,3,5-triazine (**2a**) (1.39 g, 3.50 mmol) was added and the mixture was refluxed for 18 h. The solvent was evaporated, then 1M aqueous HCl was added, then the precipitated product was collected by filtration and washed with 1M aq. HCl and $H_2O$ until the effluent was colorless. The residue was dissolved in acetone, then $CH_2Cl_2$ and aq. NaOH were added. The layers were separated, the organic layer was dried over $Na_2SO_4$, filtered, and the volatiles were thoroughly evaporated under reduced pressure to yield 2.12 g of pure **gDR1$_9$** (2.87 mmol, 90%). $T_g$ 9 °C; FTIR ($CH_2Cl_2$/KBr) 3435, 3064, 2957, 2929, 2869, 2859, 1748, 1702, 1600, 1586, 1543, 1533, 1490, 1428, 1391, 1337, 1273, 1228, 1193, 1134, 1103, 1073, 997, 856, 821, 808, 756, 736, 695 $cm^{-1}$; $^1H$ NMR (400 MHz, DMSO-$d_6$, 363 K) δ 8.31 (d, *J* = 9.1 Hz, 2H), 7.90 (d, *J* = 9.1 Hz, 2H), 7.83 (d, *J* = 9.2 Hz, 2H), 7.29 (m, 4H), 7.13 (t, *J* = 6.5 Hz, 1H), 6.94 (d, *J* = 9.2 Hz, 2H), 4.29 (t, *J* = 5.7 Hz, 2H), 3.76 (t, *J* = 5.7 Hz, 2H), 3.56 (m, 6H), 3.37 (s, 3H), 3.35 (m, 8H), 1.45 (m, 4H), 1.21 (m, 7H), 0.85 (t, *J* = 7.2 Hz, 3H) ppm; $^{13}C$ NMR (100 MHz, DMSO-$d_6$) δ 164.7, 164.4, 164.1, 156.1, 154.3, 151.7, 146.7, 144.7, 142.7, 127.8, 126.0, 125.9, 124.7, 124.4, 122.3, 111.6, 62.4, 48.2, 45.9, 45.6, 44.4, 43.1, 42.2, 36.6, 29.5, 19.4, 13.6, 11.9 ppm; UV-Vis ($CH_2Cl_2$): $\lambda_{max}$ (ε) 485 nm (41 500); HRMS (ESI) m/z: $[M + H]^+$ calcd. for $C_{39}H_{52}N_{11}O_4$: 738.4198, found: 738.4185.

**Synthesis of gDR1$_{35}$.** gDR1$_{35}$ was synthesized from Disperse Red 1 and 2-dibutylamino-4-mexylamino-6-(2-aminoethylamino)-1,3,5-triazine (**2b**) using the same procedure as **gDR1$_9$**. Yield: 85 %; $T_g$ 35 °C; FTIR ($CH_2Cl_2$/KBr) 3396, 3308, 3098, 2956, 2928, 2871, 1716, 1600, 1586, 1541, 1515, 1423, 1377, 1336, 1310, 1243, 1195, 1132, 1103, 857, 834, 821, 808, 688 $cm^{-1}$; $^1H$ NMR (400 MHz, DMSO-$d_6$, 363 K) δ 8.32 (d, *J* = 9.0 Hz, 2H), 8.22 (br s, 1H), 7.90 (d, *J* =9.0 Hz, 2H), 7.82 (d, *J* = 9.2 Hz, 2H), 7.35 (s, 2H), 6.90 (d, *J* = 9.2 Hz, 2H), 6.83 (br s, 1H), 6.56 (s, 1H), 6.28 (t, *J* = 5.6 Hz, 1H), 4.20 (t, *J* = 6.0 Hz, 2H), 3.67 (t, *J* = 6.0 Hz, 2H), 3.52 (m, 2H), 3.50 (m, 4H), 3.37 (q, *J* = 6.0 Hz, 2H), 3.23 (q, *J* = 6.0 Hz, 2H), 2.22 (s, 6H), 1.57 (m, *J* = 7.2 Hz, 4H), 1.32 (m, *J* = 7.4 Hz, 4H), 1.18 (t, *J* = 7.0 Hz, 3H), 0.91 (t, *J* = 7.2 Hz, 6H) ppm; $^{13}C$ NMR (100 MHz, DMSO-$d_6$) δ 165.4, 164.5, 163.8, 156.1, 151.5, 146.7, 142.7, 140.6, 136.9, 126.0, 124.9, 122.4, 116.9, 111.5, 61.0, 48.7, 46.0, 45.0, 40.3, 29.9, 29.7, 21.2, 19.8, 19.6, 13.9, 11.9 ppm; UV-Vis ($CH_2Cl_2$): $\lambda_{max}$ (ε) 485 nm (38 200); HRMS (ESI) m/z: $[M + H]^+$ calcd. for $C_{38}H_{52}N_{11}O_4$: 726.4198, found: 726.4184.

**Synthesis of gDR1$_{65}$.** gDR1$_{65}$ was synthesized from Disperse Red 1 and 2-pyrrolidinyl-4-mexylamino-6-(2-aminoethylamino)-1,3,5-triazine (**2c**) using the same procedure as **gDR1$_9$**. Yield: 81 %; $T_g$ 65 °C; FTIR ($CH_2Cl_2$/KBr) 3290, 3116, 2968, 2928, 2871, 1715, 1600, 1586, 1540, 1513, 1478, 1440, 1420, 1390, 1336, 1245, 1194, 1133, 1102, 856, 808, 752, 686, 619 cm$^{-1}$; $^1$H NMR (400 MHz, DMSO-$d_6$, 363 K) δ 8.32 (d, *J* = 9.1 Hz, 2H), 8.29 (br s, 1H), 7.90 (d, *J* = 9.1 Hz, 2H), 7.82 (d, *J* = 9.2 Hz, 2H), 7.41 (s, 2H), 6.90 (d, *J* = 9.2 Hz, 2H), 6.85 (br s, 1H), 6.55 (s, 1H), 6.37 (t, *J* = 5.7 Hz, 1H), 4.19 (t, *J* = 5.9 Hz, 2H), 3.67 (t, *J* = 5.9 Hz, 2H), 3.53 (m, 2H), 3.49 (m, 4H), 3.39 (q, *J* = 6.0 Hz, 2H), 3.22 (q, *J* = 5.9 Hz, 2H), 2.22 (s, 6H), 1.87 (m, 4H), 1.18 (t, *J* = 7.0 Hz, 3H) ppm; $^{13}$C NMR (100 MHz, DMSO-$d_6$) δ 165.6, 165.3, 163.7, 163.2, 156.1, 151.5, 146.7, 142.7, 140.6, 136.9, 126.0, 124.8, 122.4, 117.0, 111.5, 61.0, 48.7, 45.5, 45.0, 40.4, 24.8, 21.2, 11.9 ppm; UV-Vis ($CH_2Cl_2$): $\lambda_{max}$ (ε) 485 nm (30 800); HRMS (ESI) m/z: $[M + H]^+$ calcd. for $C_{34}H_{42}N_{11}O_4$: 668.3416, found: 668.3404.

### Thin Film Deposition

Solutions of the various **gDR1$_{Tg}$** were prepared at a concentration of 3% weight in $CH_2Cl_2$ and mechanically shaken for 1 hour. Each solution was then filtered through a 45-micron syringe filter. Soda lime microscope slides were cut into 3 x 3 cm$^2$ squares and thoroughly cleaned and dried. Approximately 0.2 ml of each solution was deposited on soda lime substrates and spun on a Headway Research spin coater at 1000 rpm for 20 s in order to make amorphous and optically uniform films. There was no cloudiness due to crystallization or other deformations observed on any of the films. The thickness of each film was measured using a Dektak XT surface profiler and the spin coater speed was subsequently adjusted for each compound, through trial and error, in order to obtain uniform films with an average thickness of 323 ± 16 nm. This was done in order to eliminate the effect of varying film thicknesses on the measured diffraction efficiency and to provide a fair comparison between the different compounds with only the chemical structures that was different. After deposition, all the thin films on the soda lime substrates were dried at room temperature.

### SRG Inscription

A Lloyd mirror interferometer was used to fabricate SRGs on the samples made from the different gDR1 materials. Two different continuous-wave lasers, having wavelengths of 488 nm and 532 nm, were used on identical optical set-ups that included a spatial filter, a beam collimator, a variable iris and a half-wave plate, before being incident on the Lloyd mirror interferometer, as described in previous papers. Both lasers were made circularly polarized before being incident on the azobenzene films since the addition of right and left circularly polarized beams results in a linearly polarized interference pattern where the polarization direction changes along the grating vector[31]. It was previously found that the combination of right and left circularly polarized light is the most efficient for SRG formation.[32] The laser incidence angle on the Lloyd mirror was set to produce sinusoidal gratings with an arbitrarily chosen pitch of 600 nm for all materials and the two different lasers.

### Diffraction Efficiency Measurements

The light diffraction intensity from a transmission phase grating, such as a SRG, is directly related to its modulation amplitude. Therefore, to monitor the SRG growth in real-time, a low-power probe He-Ne laser was mechanically chopped and made incident on the central portion of the thin film being irradiated by the writing half-circle of the interfering inscription laser. The probe laser covered an area of approximately 0.03 cm$^2$ while the SRG had an area of approximately 0.79 cm$^2$. The He-Ne laser was incident on the grating at an off-normal angle that was randomly chosen so that the first-order diffracted beam could be shone on a conveniently-located silicon photodetector connected to a lock-in amplifier and referenced to the chopper frequency. The probe laser and the photodetector were kept in the exact same position for each tested laser wavelength and while measuring the diffraction efficiency from all the azobenzene compounds. Furthermore, the probe laser incidence angle was chosen in a way to minimize the photodetector from capturing stray light in addition to physical barriers being placed in strategic locations on the optical table. The time-dependent signal from the first-order diffracted beam was recorded by a LabView program with the output coming from the signal magnitude as recorded by the lock-in amplifier. The photodiode was re-positioned after each SRG inscription to capture the transmitted zeroth order signal value from the lock-in amplifier. The ratio between the signals from the first and the zeroth diffraction orders yielded the diffraction efficiency, which is directly correlated with the grating depth. The entire diffraction efficiency measurements set-up was kept unchanged for all gratings presented in this work. This was done since it is known that the probe laser incidence angle and polarization can affect the diffraction efficiency. Therefore, all fabrication and measurement parameters were kept identical between all the samples in this work, except for the identity of the azo material.

### PM-IRSAS Measurements

Polarization modulation infrared structural absorption spectroscopy (PM-IRSAS) was used to measure *in situ* the laser-induced orientation and subsequent orientation relaxation of the DR1 moiety in **gDR1$_{Tg}$**. This technique measures simultaneously the time-resolved IR spectra polarized parallel ($A_p$) and perpendicular ($A_s$) to the laser polarization direction.[33] Spectra with a 4 cm$^{-1}$ resolution were measured using a Bruker Optics Vertex 70 Fourier transform IR spectrometer coupled to a home-built setup[34] that includes a KRS-5 linear polarizer (Optometrics), a photoelastic modulator (PEM-90 type II/ZS50, Hinds Instruments) to switch the polarization of the IR beam from parallel to perpendicular at 100 kHz, and a photovoltaic MCT detector (Kolmar Technologies). A lock-in amplifier (Stanford Research Systems SR830) with a 30 μs time constant and electronic filters (Frequency Devices 90TP/90IPB) were used to process the signal

 

Samples for PM-IRSAS were prepared by spin-coating 200 µL of 3% w/w solutions of each compound in dichloromethane. A G3P8 spin-coater (Specialty Coating Systems) was used at a 1000 rpm rate for 20 s. The uniform films were left in the fume hood for one day to complete solvent evaporation while covered with a petri dish to prevent film contamination. At least three samples of each compound were prepared and analyzed for reproducibility. The photo-orientation was induced by a 21 mW 488 nm diode laser (JDSU FCD488-020) with the laser beam expanded to 3.5 mm (Thorlabs GBE05-A) to overfill the area of the IR probe beam. The resulting ~200 mW/cm$^2$ beam was incident on the sample at an angle of ~20° with respect to IR probe for 1000 s, followed by 1000 s of relaxation with the laser turned off. The orientation parameter, $\langle P_2 \rangle$, was calculated as $\langle P_2 \rangle = (A_p - A_s) / (A_p + 2A_s)$. Different bands attributed to the azobenzene moiety gave similar results, so results are only shown for the 1134 cm$^{-1}$ band due to a ring deformation mode with a transition dipole moment along the azobenzene long axis.

## Results and Discussion

### Synthesis

Two DR1 glasses synthesized by our group have already been reported in the literature. The first such material, in which the triazine group is substituted with methylamino and mexylamino groups, can form hydrogen bonds and shows a high $T_g$ of 71 °C, and will be referred to thereafter as **gDR1$_{71}$**.[24] Its analogue with pyrrolidinyl and N-methylphenylamino substituents (**gDR1$_{51}$**) cannot form hydrogen bonds, and consequently shows a lower $T_g$ value of 51 °C.[28] In both cases, the DR1 glasses were synthesized from commercial Disperse Red 1 itself which is reacted sequentially with N,N'-carbonyldiimidazole (CDI) in dry DMF at ambient temperature followed by the corresponding amino-substituted triazine glasses in refluxing THF. This sequence has proven to be simple and efficient, affording the products in high yields, and not requiring chromatography for purification.

In order to access DR1 glasses with a wider range of $T_g$ values, amino-substituted glasses with different substituents were synthesized by reacting previously reported 4,6-dichloro-1,3,5-triazine precursors with the corresponding amines (Scheme 1). Consequently, 2-dibutylamino-4,6-dichloro-1,3,5-triazine was reacted with N-methylaniline and piperazine in a fashion similar to our previously published procedures[24] to yield secondary amine glass **2a**, or with 3,5-dimethylaniline and ethylenediamine to yield primary amine glass **2b**. Both glasses possess a dibutylamino headgroup, which is known to yield dramatically lower $T_g$ values when compared with the traditionally used methylamino or pyrrolidinyl groups. A third amino glass (**2c**), which is an analogue of compound **2b** but with a more rigid pyrrolinyl headgroup, was also synthesized from 2-mexylamino-4,6-dichloro-1,3,5-triazine and consecutive substitutions of the chloro groups by pyrrolidine and ethylenediamine.

**Scheme 1.** Synthesis of precursors **1**-**2**.‡

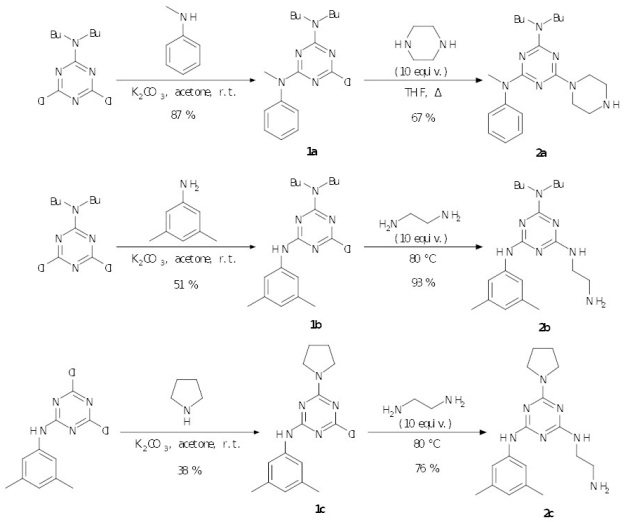


Amino glasses **2a**-**2c** were then covalently bonded to Disperse Red 1 using CDI following our previously published procedure to yield new DR1 glasses **gDR1$_9$**, **gDR1$_{35}$** and **gDR1$_{65}$** (Scheme 2). The complete structures of all five DR1 glasses used in this study are shown in Scheme 3. Again, the products were obtained in high yields (85-90 %) without requiring chromatographic purification, as all the side products and excess reagents could be removed by washing with 1M aqueous HCl. The precipitated products could then be neutralized with NaOH and extracted with $CH_2Cl_2$.

**Scheme 2.** Synthesis of DR1 glasses **gDR1$_9$**, **gDR1$_{35}$** and **gDR1$_{65}$**.

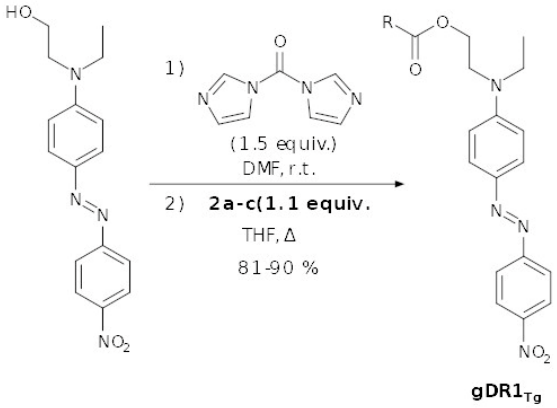

**Scheme 3.** Structures of the five DR1 glasses used in the present study.

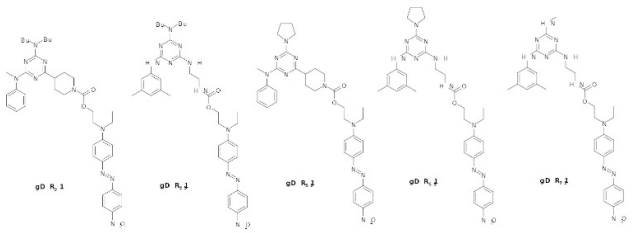

DR1 glasses **gDR1$_{35}$** and **gDR1$_{65}$** are analogues of previously reported DR1 glass **gDR1$_{71}$** where the headgroup is modified from methylamino to dibutylamino and pyrrolidinyl. On the other hand, DR1 glass **gDR1$_9$** is analogous to **gDR1$_{51}$**. These five DR1 glass thus allow to study the impact of $T_g$ (as a consequence of headgroup structure) on SRG formation. It should be noted that the structural differences between the various triazine moieties do not impact the DR1 chromophore, and the respective UV-Visible spectra of the five **gDR1$_{Tg}$** are essentially identical (Figure S3).

**Thermal Properties**

Precursor glasses **2a**-**2c** all showed the ability to form glasses upon slow cooling, with $T_g$ values measured by differential scanning calorimetry (DSC) between -29 °C for compound **2a** to 50 °C for compound **2c** (Figure S1). None of the three compounds showed any sign of crystallization upon heating by DSC at a heating rate of 5 °C/min. However, glass **2b** crystallized completely in a few weeks at ambient temperature, while glass **2a** started crystallizing slowly after a year at ambient temperature. This is likely due to the more flexible butyl chains of compounds **2a** and **2b** that can interdigit between molecules, easing the formation of ordered domains leading to crystallization, especially coupled with lower $T_g$ values. On the other hand, pyrrolidinyl glass **2c** showed no sign of crystallization upon storage, which is expected given its higher $T_g$.

DR1 glasses **gDR1$_9$**, **gDR1$_{35}$** and **gDR1$_{65}$** also showed glass forming ability, with $T_g$ values ranging, as their names indicate, from 9 °C to 65 °C (Figure S2). None of the three compounds showed any sign of crystallization upon heating or upon standing at room temperature. This is especially important with DR1 derivatives to ensure that the thin films will remain indefinitely amorphous, as crystallization would otherwise alter the surface features that will be inscribed or the SRG itself after its inscription.

**SRG Inscription and Growth**

Thin films of the various **gDR1$_{Tg}$** were deposited on soda lime microscope slides by spin-coating from 3 wt% $CH_2Cl_2$ solutions followed by drying in an oven. Amorphous thin films with thicknesses around 300 nm were thusly obtained. The resulting films were optically clear and consistent, and no cloudiness was observed due to crystallization or other deformations.

In Figure 1, the in-situ diffraction efficiency (DE) from SRGs was measured for all five DR1 glasses as a function of time upon irradiation with the 488-nm laser interference pattern at irradiances of 100, 200 and 300 mW/cm$^2$. In all cases, the DE increases with the laser exposure time, indicating successful SRG inscription. This was confirmed by Atomic Force Microscopy (AFM), as representative scans are shown for each compound in Figure S4. For **gDR1$_9$**, it must be noted that no grating is visible, this will be discussed in detail below. From the DE curves, it can be observed that there is a period of initial growth followed by a plateau when the gratings reach their maximal height. Irradiation with the 532-nm laser yields closely similar DE curves (Figure 2), with the main difference that grating growth is notably faster with the 488-nm inscribing laser, as the materials' absorbance at 488 nm is very close to their absorption maxima. For **gDR1$_{35}$**, **gDR1$_{51}$**, **gDR1$_{65}$** and **gDR1$_{71}$**, it can be observed that the SRG grow at a similar rate with irradiances of 200 or 300 mW/cm$^2$, whereas a lower irradiance (100 mW/cm$^2$) leads to a markedly slower growth. Compound **gDR1$_{71}$**, which has the highest $T_g$ value, is the only DR1 glass that shows a notably faster growth rate at 300 mW/cm$^2$ than at 200 mW/cm$^2$. This is arguably due to the higher $T_g$ of the material, which translates to lower molecular mobility of the non-photoactive triazine moieties. On the other hand, irradiation of **gDR1$_9$** with an irradiance of 300 mW/cm$^2$ resulted in an initial rise followed by a fast decay in the DE signal, which is likely a consequence of the collapse of the gratings due to local heating by the laser, as the $T_g$ of the material is sub-ambient. This effect is observed to a lower extent in the other compounds, as higher irradiances lead to lower maximal DE values in every case, with closer values as $T_g$ increases. To optimize the writing process, it would be therefore advantageous to start with a high irradiance to ensure fast initial growth, then progressively decrease the irradiance in order to reach maximal grating height and diffraction efficiency.

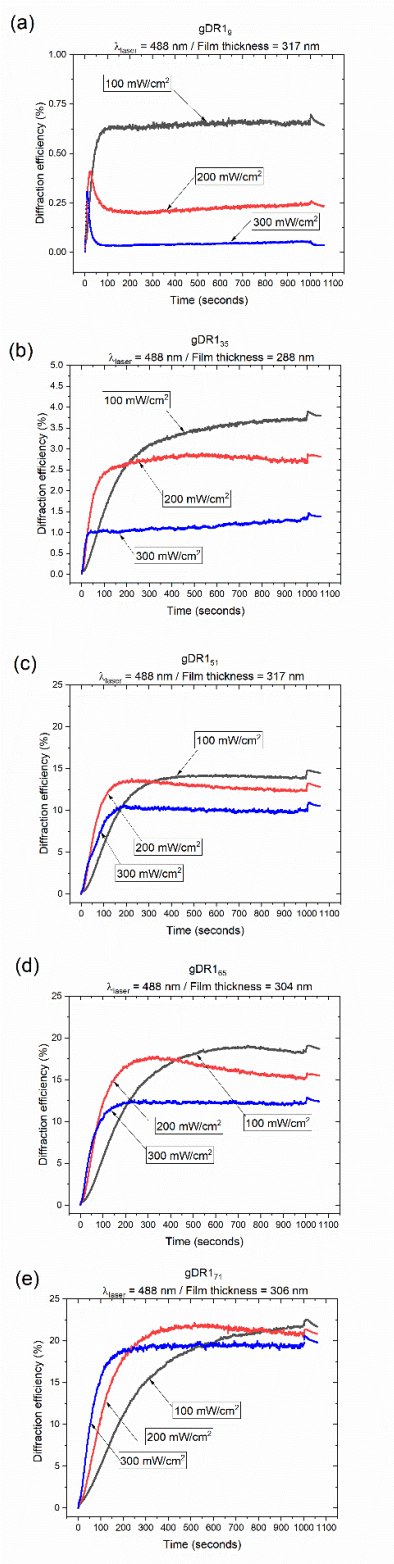


**Figure 1.** Diffraction Efficiency (DE) curves as a function of irradiation time for **gDR1$_{Tg}$** during irradiation with a 488-nm laser with irradiances of 100 (black), 200 (red) and 300 (blue) mW/cm$^2$. a) **gDR1$_9$**, b) **gDR1$_{35}$**, c) **gDR1$_{51}$**, d) **gDR1$_{65}$**, and e) **gDR1$_{71}$**.

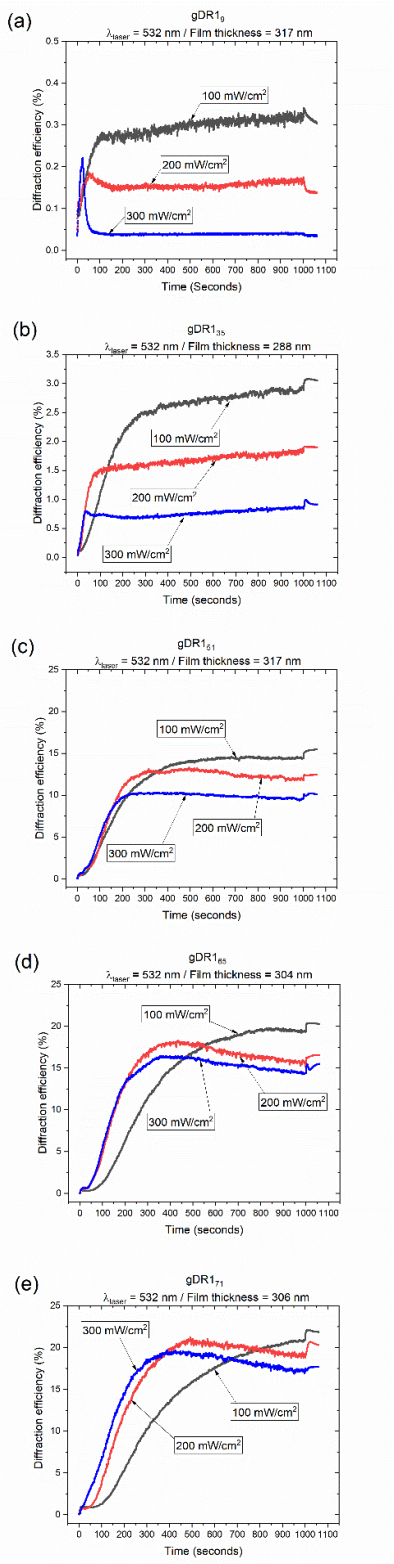


**Figure 2.** Diffraction Efficiency (DE) curves as a function of irradiation time for **gDR1$_{Tg}$** during irradiation with a 532-nm laser with irradiances of 100 (black), 200 (red) and 300 (blue) mW/cm$^2$. a) **gDR1$_9$**, b) **gDR1$_{35}$**, c) **gDR1$_{51}$**, d) **gDR1$_{65}$**, and e) **gDR1$_{71}$**.

To provide an accurate comparison between the SRG growth rates of the various **gDR1$_{Tg}$**, the times required for compounds **gDR1$_{35}$**, **gDR1$_{51}$**, **gDR1$_{65}$** and **gDR1$_{71}$** to reach a DE of 1 % and 5 % at each 532-nm laser irradiance are listed in Table 1 (**gDR1$_9$** is not included as it never reaches a DE of 1 %). As the SRG formed by the various DR1 glasses reach different maximal modulation depths (corresponding to different DE values), these DE values allow a uniform comparison of all four compounds as DE has not reached a plateau at this stage. It should be noted that the growth rates of the gratings with the 488-nm laser were so fast that the differences between compounds **gDR1$_{51}$**, **gDR1$_{65}$** and **gDR1$_{71}$** were merely statistical.

**Table 1.** Times required to reach diffraction efficiency (DE) values of 1% and 5% for **gDR1$_{Tg}$** upon irradiation with a 532-nm laser.

| gDR1$_{Tg}$ | Irradiance (mW/cm$^2$) | t (1%) (s) | t (5%) (s) |
|---|---|---|---|
| **gDR1$_{35}$** | 100 | 95 | |
| | 200 | 40 | |
| | 300 | 35[a] | |
| **gDR1$_{51}$** | 100 | 47 | 120 |
| | 200 | 31 | 110 |
| | 300 | 30 | 100 |
| **gDR1$_{65}$** | 100 | 89 | 179 |
| | 200 | 43 | 104 |
| | 300 | 44 | 96 |
| **gDR1$_{71}$** | 100 | 76 | 192 |
| | 200 | 50 | 114 |
| | 300 | 15.4 | 79 |

[a] The DE value reaches a maximum of 0.8% at the given time.

It can be observed that **gDR1$_{51}$** tends to show the fastest SRG growth at lower laser irradiances (100-200 mW/cm$^2$) but not at the highest irradiance (300 mW/cm$^2$), where **gDR1$_{71}$** shows faster growth. This is likely due to the fact that higher irradiance causes more softening in the materials through photoplasticization, thereby increasing molecular mobility in the material.[31] The initial growth rates have been also calculated from the slopes of the linear portions of the curves (Tables S1-S2) and mostly mirror the trends observed in Table 1 with the 532 nm laser. With the 488 nm laser, similar trends are observed, except for **gDR1$_{51}$** showing a substantially faster growth rate at 200 mW/cm$^2$ than at 300 mW/cm$^2$. It must be noted that these inital growth rates do not take into account the induction time that is often present, especially in **gDR1$_{65}$** and **gDR1$_{71}$**, and which contributes to delay SRG growth. In fact, the most important factor contributing to increase the inscription speed in **gDR1$_{71}$** is the decrease in induction time when increasing laser irradiance. The optimal $T_g$ for SRG growth thus increases with laser irradiance, as it is dependent on molecular mobility in the materials under irradiation. In materials with $T_g$ higher than the optimal values, the rigidity of the backbone will cause a slower migration of the azobenzene moieties, whereas in materials with lower $T_g$ values, photoplasticization promotes molecular relaxation and thus limits SRG growth. This is consistent with the previous demonstration, using mixtures of **gDR1$_{71}$**, that a $T_g$ range between 50 °C and 60 °C is optimal for the rapid growth of SRG when using an irradiance of 230 mW/cm$^2$.[27] Besides growth speed, the maximal SRG modulation depth that can be attained is also an important parameter to consider, as grating depth can be important for some applications, including optical waveguides and plasmonic sensors. As grating depth is directly correlated with DE, the DE values for each grating at a constant irradiation time of 800 s are listed in Table 2. At this time, all gratings have reached equilibrium, thereby allowing an accurate comparison of their respective depths.

**Table 2.** Diffraction efficiency (DE) values at an irradiation time of 800 s for **gDR1$_{Tg}$** upon irradiation with a 488-nm or a 532-nm laser.

| gDR1$_{Tg}$ | Irradiance (mW/cm$^2$) | DE (488 nm) (%) | DE (532 nm) (%) |
|---|---|---|---|
| **gDR1$_9$** | 100 | 0.7 | 0.3 |
| | 200 | 0.2 | 0.2 |
| | 300 | 0.1 | 0.04 |
| **gDR1$_{35}$** | 100 | 3.6 | 2.8 |
| | 200 | 2.8 | 1.7 |
| | 300 | 1.2 | 0.8 |
| **gDR1$_{51}$** | 100 | 14.0 | 14.5 |
| | 200 | 12.6 | 12.2 |
| | 300 | 10.1 | 9.9 |
| **gDR1$_{65}$** | 100 | 18.8 | 19.6 |
| | 200 | 15.7[a] | 16.3[b] |
| | 300 | 12.3 | 14.8[c] |
| **gDR1$_{71}$** | 100 | 21.0 | 19.9 |
| | 200 | 21.1 | 19.4 |
| | 300 | 19.4 | 17.9[d] |

[a] 17.4 % at 272 s. [b] 18.2 % at 438 s. [c] 16.3 % at 385 s. [d] 19.5 % at 406 s.

As it can be observed from Table 2, maximal DE increases with $T_g$, and decreases with increasing laser power, though the impact of laser irradiance is mitigated in materials with higher $T_g$. These observations are also consistent with the explanation that due to local heating from the laser coupled with the photoplasticization associated with azo isomerization-induced excess free volume, partial thermal relaxation and photomechanical SRG collapse will occur in materials, which is exacerbated when the $T_g$ of the materials is close to ambient temperature.

Compound **gDR1$_9$** presents an interesting case as it shows a sub-ambient $T_g$ (9 °C); it is already in the viscous state at ambient temperature, though its viscosity is still high. Its sub-ambient $T_g$, which is so far unique among azo glasses or polymers, coupled with its high resistance to crystallization, may lead to the formation of transient gratings that form when the material is irradiated but collapse when irradiation is stopped. Indeed, it can be observed from Figure 3 that when the DE is still monitored after irradiation is stopped, the DE decays gradually, to reach 25 % of its initial value after 1000 s. In contrast, the DE reaches its plateau value within a few seconds upon irradiation. Repeated on-off irradiation cycles yield consistent behavior. An azo polysiloxane with a $T_g$ of 25 °C has been previously reported to form unstable SRG that eventually disappeared.[35] However, the gratings started erasing after an hour, and remnants of

gratings were still visible by AFM two weeks after inscription. In the present case, erasure is completed after 20 minutes, and no visible trace of the gratings is visible by AFM after two hours (Figure S4). Despite the relatively long time required for the gratings to fully collapse as compared to the inscription time, this constitutes a substantial step towards designing self-healing and self-modifying materials, which could lead to various optical devices taking advantage of the temporary nature of the inscribed SRG. These include optical switches, as well as transient light filters and diverters that can be used in communications.[36] Since it has been shown in the past that non-uniform gratings can also be inscribed on azobenzene films,[37] these gratings are in fact holographic representations of the phase and amplitude of the inscribing laser beam interference pattern.[38] Therefore, self-erasable non-uniform SRG can be used in dynamic holographic displays.

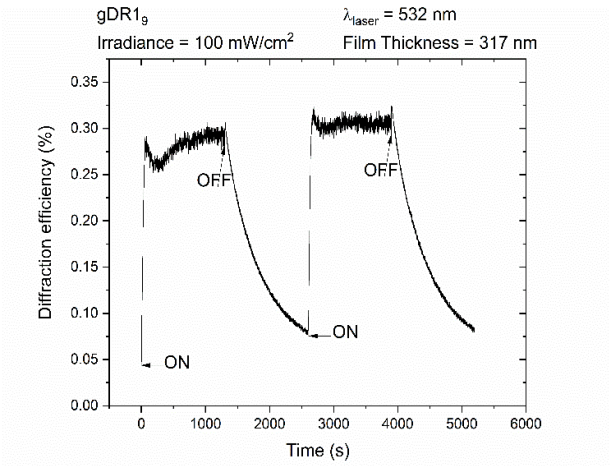


**Figure 3.** Diffraction efficiency (DE) of gDR1$_9$ under repeated on-off irradiation cycles with a 532-nm laser at an irradiance of 100 mW/cm$^2$.

Infrared spectroscopy measurements of photoinduced orientation were conducted to provide molecular insight on the role of $T_g$ in the SRG inscription process. Our previous work on mixtures of **gDR1$_{71}$** with various passive glasses has revealed that the propensity of the azobenzene to orient under linearly polarized irradiation and the stability of the orientation vary greatly with the $T_g$ of the mixture and correlate with the SRG inscription rate and saturated DE values, respectively.[27] Samples of **gDR1$_{Tg}$** were thus irradiated with 488 nm laser light of 200 mW/cm$^2$ to determine if these correlations hold for the pure azo glasses. Figure 4a shows representative orientation and relaxation curves for the 5 compounds, where orientation parameters (or $<P_2>$ values) are negative because of perpendicular orientation of the azo with respect to the laser polarization. In all cases, the orientation grows extremely rapidly when turning on the laser, in part due to the fast process of angular hole burning (AHB), and a quasi-plateau is reached within approximately 5 s. This is consistent with the very rapid initial rise of DE typically present at the onset of SRG inscription and most easily seen in Figure 1 with 488-nm laser irradiation. However, it is clear that most of the SRG builds during the orientation quasi-plateau, where angular reorientation (AR) perpendicular to the laser polarization due to trans-cis-trans cycling is in dynamic dissipative equilibrium with the rotational diffusion (RD) process that tends to return the sample to an isotropic state.

Increasing the $T_g$ of the compound leads to higher saturated orientation, $<P_2>_{sat}$. Indeed, a higher $T_g$ increases the viscosity of the material and reduces the rate of RD that is detrimental to high orientation. The $<P_2>_{sat}$ reached is slightly higher than what was previously obtained for mixtures of **gDR1$_{71}$** with a similar $T_g$. In particular, compound **gDR1$_9$** reaches a $<P_2>_{sat}$ value of -0.050 ± 0.001, which is significant, while the previously studied mixtures with a $T_g$ of 22 or 19 °C presented $<P_2>_{sat}$ very close to zero. The dilution (only 10 mol%) of the photoactive azo glass in a passive matrix thus appears to restrict its capacity to orient, especially at low $T_g$, possibly due to a lack of cooperative intermolecular interactions between the DR1 units. Unfortunately, it was not possible to validate the previously observed correlation between the SRG inscription rate and $<P_2>_{sat}$ because of the above-mentioned difficulty in quantifying the DE growth rate. Nevertheless, the observation in Figures 1-2 of a low but meaningful DE for the low-$T_g$ compounds is, at least, consistent with the role of molecular orientation in the inscription rate. Also, the unexpectedly similar orientation of compound **gDR1$_{51}$** compared to **gDR1$_{65}$** (-0.100 ± 0.001 and -0.098 ± 0.001), may relate to the above-mentioned SRG writing efficiency of the former.

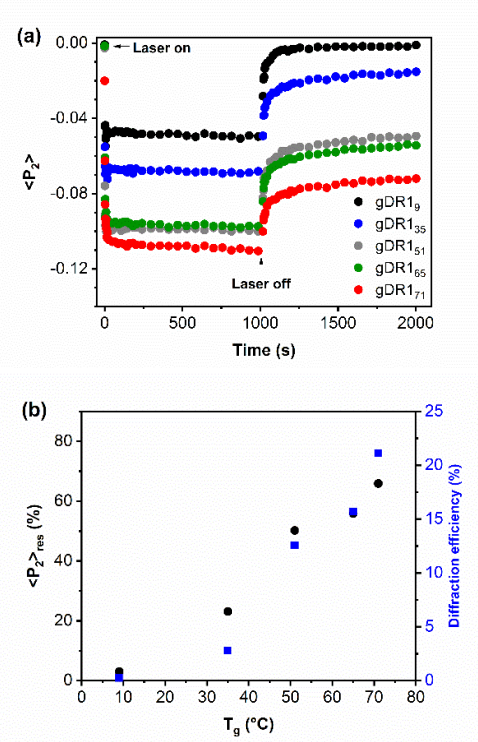


**Figure 4.** a) Orientation parameters ($<P_2>$) for gDR1$_{Tg}$ during and after (laser off) irradiation with a 488-nm laser with an irradiance of 200 mW/cm$^2$; and b) residual orientation parameters ($<P_2>_{res}$) and maximal diffraction efficiency (DE) of gDR1$_{Tg}$ as a function of $T_g$.

Figure 4a also shows that once the laser is turned off, the orientation relaxes to an extent that strongly depends on $T_g$. Two main processes are involved. First, a fast relaxation process occurs over 20-30 s where approximately 0.015 to 0.020 orientation units are lost for all compounds, irrespective of their $T_g$ or $\langle P_2 \rangle_{sat}$ reached under irradiation. This fast process was assigned to the reversal of the AHB process where the cis conformers return to trans conformation.[34] This is followed by a much slower relaxation process related to RD, where the photoinduced orientation is gradually erased by thermally activated motions of the matrix. This process depends on $T_g$ and is much longer than the 1000 s experimental time scale for compounds with a high $T_g$. The relative importance of the relaxation can be expressed by the $\langle P_2 \rangle_{res}$ values, which are calculated as the percentage of the $\langle P_2 \rangle$ values at the end of the 1000-s relaxation with respect to $\langle P_2 \rangle_{sat}$. Figure 4b shows that $\langle P_2 \rangle_{res}$ increases gradually with $T_g$, consistent with the increasing viscosity of the matrix. The values are in good agreement with the results obtained on mixtures (Figure S5). Importantly, the $\langle P_2 \rangle_{res}$ values correlate well with the maximum DE values reached for the SRG inscribed under similar irradiation conditions (488 nm, 200 mW/cm$^2$), confirming that the capability to write deep SRG with high DE is connected to a high stability of the azobenzene orientation. These results further inform on the unusual behavior of compound **gDR1$_9$**. With a sub-ambient $T_g$ of 9 °C, the orientation measured for this compound is dominated by AHB, which enables the rapid inscription of a transient volume grating during the SRG experiment. However, the relaxation results indicate that some orientation by also occurred by the AR proceed, thus enabling a "semi-permanent" grating to be inscribed. Once the laser is turned off, the low viscosity of the material enables a fast orientation relaxation and a relatively fast self-erasure of the grating as illustrated in Figure 3.

## Conclusions

Three new analogous molecular glasses incorporating the Disperse Red 1 chromophore with glass transition temperatures ($T_g$) ranging from 9 to 65 °C were synthesized. These azobenzene glasses, along with two previously published analogues, allow a comparison of their respective surface relief grating (SRG) growth rates, to better understand the impact of the $T_g$ of the materials on SRG growth. SRG were grown on thin films using two different laser wavelengths (488 and 532 nm) at three different irradiances (100, 200 and 300 mW/cm$^2$). The $T_g$ allowing for optimal SRG growth rate was found to increase as a function of laser irradiance, from approximately 50 °C at 100 mW/cm$^2$ to over 70 °C at 300 mW/cm$^2$. This is likely due to the photoplasticization resulting from cis-trans isomerization cycles in the azobenzene moieties, with higher laser irradiances causing faster isomerization, and consequently a higher molecular mobility in the materials. The maximum diffraction efficiency reached by the SRG gradually increases with $T_g$ and correlates with the stability of the light-induced molecular orientation of the azobenzene.

Interestingly, the material with a sub-ambient $T_g$ of 9 °C was found to form SRG that spontaneously erase when irradiation is stopped, a consequence of its lower viscosity at ambient temperature. This constitutes a first step towards the design of light-controlled optical devices. Such materials could be used in the future for optical switches, light filters and diverters, and dynamic holographic displays.

## Acknowledgements

The authors thank the Natural Sciences and Engineering Research Council (NSERC # RGPIN-2015-05743 (RGS) and RGPIN-04014-2015 (CP)) and the Canadian Defence Academy Research Programme (CDARP) from RMC for funding.

## Notes and references

‡ Marvin was used for drawing, displaying and characterizing chemical structures, substructures and reactions, Marvin 17.26, 2017, ChemAxon (www.chemaxon.com).

1. S. L. Oscurato, M. Salvatore, P. Maddalena and A. Ambrosio, *Nanophotonics*, 2018, **7**, 1387-1422.
2. C. J. Barrett, P. L. Rochon and A. L. Natansohn, *J. Chem. Phys*, 1998, **109**, 1505-1516.
3. P. Rochon, E. Batalla and A. Natansohn, *App. Phys. Lett.*, 1995, **66**, 136-138.
4. S. Bian, J. M. Williams, D. Y. Kim, L. Li, S. Balasubramanian, J. Kumar and S. Tripathy, *J. Appl. Phys.*, 1999, **86**, 4498-4508.
5. A. Natansohn and P. Rochon, *Chem. Rev.*, 2002, **102**, 4139-4176.
6. Y.-B. Wei, Q. Tang, C.-b. Gong and M. H.-W. Lam, *Anal. Chim. Acta*, 2015, **900**, 10-20.
7. Y. Shirota and H. Kageyama, *Chem. Rev.*, 2007, **107**, 953-1010.
8. Y. Shirota, *J. Mat. Chem.*, 2005, **15**, 75-93.
9. Y. Shirota, *J. Mat. Chem.*, 2000, **10**, 1-25.
10. P. Strohriegl and J. V. Grazulevicius, *Adv. Mater.*, 2002, **14**, 1439-1452.
11. M. D. Ediger, C. A. Angell and S. R. Nagel, *J. Phys. Chem.*, 1996, **100**, 13200-13212.
12. L. Berthier and M. D. Ediger, *arXiv preprint arXiv:1512.03540*, 2015.
13. H. Nakano, T. Takahashi, T. Kadota and Y. Shirota, *Adv. Mat.*, 2002, **14**, 1157-1160.
14. E. Ishow, R. Camacho-Aguilera, J. Guérin, A. Brosseau and K. Nakatani, *Adv. Funct. Mat.*, 2009, **19**, 796-804.
15. E. Ishow, B. Lebon, Y. He, X. Wang, L. Bouteiller, L. Galmiche and K. Nakatani, *Chem. Mat.*, 2006, **18**, 1261-1267.
16. H. Nakano, T. Takahashi, T. Tanino and Y. Shirota, *Dyes and Pigm.*, 2010, **84**, 102-107.
17. H. Nakano, T. Tanino, T. Takahashi, H. Ando and Y. Shirota, *J. Mater. Chem.*, 2008, **18**, 242-246.
18. A. Jacquart, E. Morin, F. Yang, B. Geffroy and E. Ishow, *Pigm.*, 2012, **92**, 790-797.
19. K. E. Snell, R. Hou, E. Ishow and F. Lagugné-Labarthet, *Langmuir*, 2015, **31**, 7296-7305.
20. T. Fuhrmann and T. Tsutsui, *Chem. Mater.*, 1999, **11**, 2226-2232.

 

21. M.-J. Kim, E.-M. Seo, D. Vak and D.-Y. Kim, *Chem. Mater.*, 2003, **15**, 4021-4027.
22. K. Traskovskis, I. Mihailovs, A. Tokmakovs, A. Jurgis, V. Kokars and M. Rutkis, *J. Mater. Chem.*, 2012, **22**, 11268-11276.
23. O. R. Bennani, T. A. Al-Hujran, J.-M. Nunzi, R. G. Sabat and O. Lebel, *New J. Chem.*, 2015, **39**, 9162-9170.
24. R. Kirby, R. G. Sabat, J.-M. Nunzi and O. Lebel, *J. Mater. Chem. C*, 2014, **2**, 841-847.
25. K. G. Yager and C. J. Barrett, *Macromolecules*, 2006, **39**, 9320-9326.
26. Y. Zhao and T. Ikeda, *Smart light-responsive materials: azobenzene-containing polymers and liquid crystals*, John Wiley & Sons, 2009.
27. A. Laventure, J. Bourotte, J. Vapaavuori, L. Karperien, R. G. Sabat, O. Lebel and C. Pellerin, *ACS Appl. Mater. & Interfaces*, 2017, **9**, 798-808.
28. A. Tofini, L. Levesque, O. Lebel and R. G. Sabat, *J. Mater. Chem. C*, 2018, **6**, 1083-1091.
29. J. A. Carbon and S. H. Tabata, *J. Org. Chem.*, 1962, **27**, 2504-2509.
30. Y. Zhou, Z. Sun, J. M. Froelich, T. Hermann and D. Wall, *Bioorg. Med. Chem. Lett.*, 2006, **16**, 5451-5456.
31. N. S. Yadavalli, M. Saphiannikova and S. Santer, *Appl. Phys. Lett.*, 2014, **105**, 051601.
32. N. K. Viswanathan, S. Balasubramanian, L. Li, S. K. Tripathy and J. Kumar, *Jap. J. Appl. Phys.*, 1999, **38**, 5928.
33. Y. Liang, D. Mauran, R. E. Prud'Homme and C. Pellerin, *Appl. Spectr.*, 2008, **62**, 941-947.
34. X. Wang, J. Vapaavuori, C. G. Bazuin and C. Pellerin, *Macromolecules*, 2018, **51**, 1077-1087.
35. V. Damian, E. Resmerita, I. Stoica, C. Ibanescu, L. Sacarescu, L. Rocha and N. Hurduc, *J. Appl. Poly. Sci.*, 2014, **131**.
36. R. J. Stockermans and P. L. Rochon, *Appl. Opt.*, 1999, **38**, 3714-3719.
37. N. Swanson and R. G. Sabat, *Opt. Expr.*, 2018, **26**, 7876-7887.
38. F. Lagugné Labarthet, T. Buffeteau and C. Sourisseau, *J. Phys. Chem. B*, 1998, **102**, 2654-2662.